Role of electronic localization in the phosphorescence of iridium sensitizing dyes

Burak Himmetoglu,[1] Alex Marchenko*,[1,2] Ismaïla Dabo,[3] and Matteo Cococcioni[1]

[1]*Department of Chemical Engineering and Materials Science, University of Minnesota, Minneapolis, MN, 55455, USA*
[2]*Department of Chemistry, University of Minnesota, Minneapolis, MN, 55455, USA*
[3]*CERMICS, Université Paris-Est, Champus sur Marne 77455 Marne la Vallee Cedex 2, France*

(Dated: September 18, 2012)

In this work we present a systematic study of three representative iridium dyes, namely, $Ir(ppy)_3$, FIrpic and PQIr, which are commonly used as sensitizers in organic optoelectronic devices. We show that electronic correlations play a crucial role in determining the excited-state energies in these systems, due to localization of electrons on Ir *d* orbitals. Electronic localization is captured by employing hybrid functionals within time-dependent density-functional theory (TDDFT) and with Hubbard-model corrections within the Δ-SCF approach. The performance of both methods are studied comparatively and shown to be in good agreement with experiment. The Hubbard-corrected functionals provide further insight into the localization of electrons and on the charge-transfer character of excited-states. The gained insight allows us to comment on envisioned functionalization strategies to improve the performance of these systems. Complementary discussions on the Δ-SCF method are also presented in order to fill some of the gaps in the literature.

I. INTRODUCTION

Phosphorescent organometallic dyes have attracted considerable interest over the last few decades as highly efficient sensitizers in organic light-emitting diodes (OLEDs) [1]. These complexes are characterized by strong spin-orbit coupling due to heavy transition metals in their core, such as Ir, Pt, and Os. The strong spin-orbit coupling leads to intersystem crossing from the singlet to triplet excited states and allows for the emission from the otherwise forbidden triplet state (phosphorescence), in addition to emission from the singlet state (fluorescence). As a result, phosphorescent emitters can have an internal quantum efficiency of 100% [1]. Moreover, the possibility to tune the colors of these emitters by modifications in the ligands surrounding the transition-metal center has opened up the possibility to design color displays and efficient white light sources from organic materials (see Ref. 2 for a review).

More recently, the strong intersystem-crossing mechanism that take place in these complexes have been exploited to design organic solar cells (OSCs) of improved power conversion efficiency [3, 4]. In fact, in organic heterojunctions, sensitizing transition-metal complexes are utilized as promoters in converting photogenerated singlet excitons into long-lived triplet excitons, thereby increasing the probability for an exciton to diffuse to a donor-acceptor interface and dissociate into collectible charges [3, 4]. In a recent study [3] it was reported that incorporating $Ir(ppy)_3$ (in concentrations as low as few mass percents) into electron-donating polymers nearly doubled the photovoltaic efficiency of the considered organic heterojunctions.

These remarkable experimental achievements motivate further theoretical effort to understand the optical properties of transition-metal complexes and ultimately optimize their sensitizing functions taking advantage of their almost unlimited chemical versatility, i.e., modifying the transition-metal center and attached chromophores. To assist in this endeavor, computational methods of increasing predictive ability are now available. Among successful electronic-structure techniques, the Green's function many-body perturbation theory (GW) with Bethe-Salpeter post-treatment has been accurate in predicting excited-state energies [5, 6], yet requiring considerable effort to achieve full self-consistent convergence. Computationally less demanding predictions are based upon time-dependent density-functional theory (TDDFT) and linear-response theory [7–9]. Recently, alternative Δ-SCF [10] techniques that consist in evaluating excited-state energies from moderately demanding constrained density-functional theory (DFT) calculations have also seen a revival of interest [11–13].

In spite of their limited cost, the accuracy of TDDFT and Δ-SCF approximations depends crucially on the ability of the underlying DFT functional to properly capture orbital localization. In this regard, local and semilocal DFT functionals are known to insufficiently localize electronic states. Moreover, conventional TDDFT calculations rely on the adiabatic approximation whereby the frequency dependence of the TDDFT kernel is neglected, representing another important source of error in capturing excited states. In practical terms, TDDFT approximations do not properly describe charge-transfer states that consist of an electron weakly coupled to a hole [14–21].

In this study, we examine the performance of TDDFT and Δ-SCF approximations in predicting singlet and triplet excitonic energies in three representative Ir complexes, namely, $Ir(ppy)_3$, FIrpic and PQIr, which emit in the green, the blue and the red [22], respectively.

*present adress: Nuclear Engineering and Materials Science, Universitat Politècnica de Catalunya, Barcelona, Spain

Specifically, we compare TDDFT with Δ-SCF that employ Hubbard corrections, enabling us to gain needed insight into the effects of electronic localization and charge-transfer for excited states and comment on envisioned functionalization strategies. Such insight will be useful to study the influence of ligand modification on singlet and triplet energies with the ultimate goal of guiding experiments in designing more efficient OLEDs and OSCs.

The paper is organized as follows: We provide some technical details about the computational approach used in this work in Section II and summarize the methods employed to compute excited-state energies within TDDFT and Δ-SCF in Section III. In Section IV, we present the main results and provide a detailed discussion on the performance of the methods used and some comments on strategies to tune excited-state energies. Finally, we provide some concluding remarks. We also include an Appendix, which provides a brief analysis of the calculation of the singlet excited-state energy, within the Δ-SCF approach.

II. COMPUTATIONAL METHODS

Structural optimizations and Δ-SCF calculations presented in this paper were performed using the plane-waves pseudopotential implementation of DFT contained in the PWSCF code of the *Quantum ESPRESSO* package [23]. The TDDFT calculations were performed using the *Gaussian 09* package [24]. For plane-wave calculations, the exchange-correlation energy was approximated using the generalized-gradient approximation (GGA) with the Perdew-Burke-Ernzherof (PBE) parametrization [25]. The Ir, N, C, and H atoms were all represented by ultrasoft pseudopotentials [26]. The electronic wavefunctions and charge density were expanded up to kinetic energy cutoffs of 30 Ry and 360 Ry, respectively. In performing TDDFT calculations, the SDD basis set of Refs. 27–33 was used. The semilocal PBE [25] and hybrid functionals B3LYP [34, 35] and M06 [36] were used in the TDDFT calculations.

In our plane wave calculations, we employed the Hubbard-model corrected DFT+U [37–40] method, in order to capture the effects of electronic localization accurately. An improved version of the DFT+U formalism, which includes inter-site interactions (DFT+U+V) [41], was also used in order to obtain a better description of interactions between localized electrons on Ir d states and the surrounding organic ligands. The values of the Coulomb interaction parameters U and V were computed using the linear-response method introduced in Ref. 40. The molecular structures and charge densities presented in this paper were generated using XCrysden [42].

III. THEORETICAL OVERVIEW

In this section, we provide a brief overview of the computational approaches used in this paper. We refer the reader to the original literature for a complete discussion of these methods.

A. TDDFT

The theorem of Runge and Gross [7] states that there is a one-to-one correspondence between a time-dependent external potential and the electronic density of a many-body system. A particular application of the Runge-Gross theorem was used to compute the energies of excited states of many-body systems, using linear-response functions [8, 9]. Within this approach, the poles of the response function provide the excited-state energies of the system, which can be determined through the solution of the following eigenvalue problem [9, 27–33]:

$$\begin{pmatrix} \mathbf{L} & \mathbf{M} \\ \mathbf{M}^* & \mathbf{L}^* \end{pmatrix} \begin{pmatrix} \mathbf{X}(\omega) \\ \mathbf{Y}(\omega) \end{pmatrix} = \omega \begin{pmatrix} -\mathbf{I} & 0 \\ 0 & \mathbf{I} \end{pmatrix} \begin{pmatrix} \mathbf{X}(\omega) \\ \mathbf{Y}(\omega) \end{pmatrix} \quad (1)$$

where the solutions ω represent excited-state energies. The matrices $\mathbf{L}$ and $\mathbf{M}$ are given by

$$\begin{aligned} L_{i\,a\,\sigma;j\,b\,\tau} &= \delta_{\sigma\,\tau}\,\delta_{i\,j}\,\delta_{a\,b}\,(\epsilon_a^\sigma - \epsilon_i^\sigma) + M_{i\,a\,\sigma;b\,j\,\tau} \\ M_{i\,a\,\sigma;j\,b\,\tau} &= \int d^3\mathbf{r} \int d^3\mathbf{r}'\, \psi_i^{\sigma *}(\mathbf{r})\, \psi_a^\sigma(\mathbf{r}) \\ &\quad \times K^{\sigma\,\tau}(\mathbf{r},\mathbf{r}')\, \psi_j^{\tau *}(\mathbf{r}')\, \psi_b^\tau(\mathbf{r}), \\ K^{\sigma\,\tau}(\mathbf{r},\mathbf{r}') &= \frac{1}{|\mathbf{r}-\mathbf{r}'|} + \frac{\delta^2 E_{\rm xc}}{\delta\rho_\sigma(\mathbf{r})\,\delta\rho_\tau(\mathbf{r}')} \end{aligned} \quad (2)$$

where ψ_i^σ are solutions to the Kohn-Sham (KS) equations with eigenvalues ϵ_i^σ, $E_{\rm xc}$ is the exchange-correlation functional, and ρ_σ denotes the single-particle density constructed from occupied Kohn-Sham states. In addition, we adopt the convention that the indices i, j run over occupied states, while a, b run over unoccupied states, and the frequency-dependent vector coefficients $X_{i\,a\,\sigma} = Y_{a\,i\,\sigma}$ are related to the response of the electronic density to a time-dependent perturbation through

$$\delta\rho_\sigma(\mathbf{r},t) = \int d\omega \sum_{i,\,a} \left[X_{i\,a\,\sigma}(\omega)\, \psi_a^{\sigma *}(\mathbf{r})\, \psi_i^\sigma(\mathbf{r})\, e^{-i\omega t} + (a \leftrightarrow i) \right] \quad (3)$$

Very often, the frequency dependence of the approximate exchange-correlation functional $E_{\rm xc}$ is ignored (the adiabatic approximation), in obtaining solutions to Eq. (1). It is well known that the approach briefly summarized above usually fails in reproducing experimental excited-state energies for Rydberg and charge-transfer-type excitations [14–21]. In charge-transfer excitations, the occupied ψ_i^σ and unoccupied ψ_a^σ orbitals are spatially separated. Therefore, the matrix $\mathbf{M}$, representing the off-diagonal block in Eq. (1) becomes negligible for local or semilocal exchange-correlation functionals (such as

PBE), while **L** reduces to a diagonal matrix composed of energy differences of occupied and unoccupied KS states. As a result, the excitation energies are simply given by KS energy differences, which underestimate the experimental values [14]. This inaccuracy can be corrected to some extent with the use of nonlocal, hybrid functionals (such as B3LYP and M06). The inaccuracy related to Rydberg and charge-transfer type excitations stems from the incorrect asymptotic behavior of most approximate exchange-correlation functionals, and can be mitigated by improving their long-range behavior [19, 21, 43–50]. The modifications to the long-range interactions are generally parameterized and determined empirically. Alternatively, they can be determined from first-principles in a system-dependent fashion [51–53]. Several works also considered the Δ-SCF method (discussed in the next subsection) to be more precise for these types of excitations compared to TDDFT [11–13, 18]. A mixture of the two approaches has also been shown to be effective in treating charge-transfer excitations [54, 55].

B. Δ-SCF

Δ-SCF method is based on the construction of excited-state electronic densities, using a non-Aufbau scheme for orbital occupations [10]. For a system of N electrons, the electronic density is constructed by filling the lowest $N-1$ orbitals and the $(N+1)^{\text{th}}$ orbital at each iteration of the electronic-structure optimization until self-consistency is reached. More precisely, the electronic density of an excited-state of spin σ is given by

$$\rho_\sigma^{\text{ex}}(\mathbf{r}) = \sum_{i=1}^{N-1} |\psi_i^\sigma(\mathbf{r})|^2 + |\psi_{N+1}^\sigma(\mathbf{r})|^2 \tag{4}$$

where the orbitals ψ_i^σ are self-consistently determined from the minimization of the energy functional depending on the density in Eq.(4). Examples of such configurations are schematically represented in Fig. 1, where the ground-state is assumed to be in a closed shell configuration. The constructed density can be reproduced from a single excited Slater determinant of specific space and spin symmetry (for some cases). In Fig. 1, Φ_{G} refers to

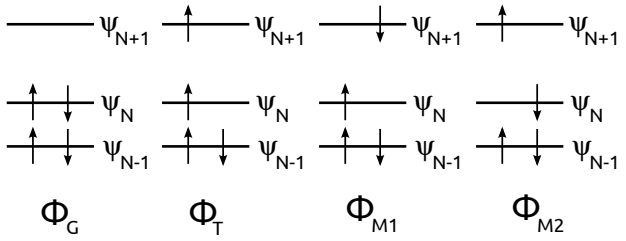

FIG. 1: Schematic representation of the single determinant configurations used in Δ-SCF calculations

the ground-state wavefunction, Φ_{T} is a triplet excited-state, while Φ_{M1} and Φ_{M2} are excited-states with mixed spin symmetry. For the moment, orbital relaxation due to KS self-consistency is ignored. The spin symmetries of these states can be explicitly determined through the action of the spin operators $\vec{S}^2$ and S_z, which yields (ignoring orbital relaxations),

$$\begin{aligned}
&\vec{S}^2\,|\Phi_{\text{G}}\rangle = 0, \quad S_z\,|\Phi_{\text{G}}\rangle = 0\\
&\vec{S}^2\,|\Phi_{\text{T}}\rangle = 2\,|\Phi_{\text{T}}\rangle, \quad S_z\,|\Phi_{\text{T}}\rangle = 1\,|\Phi_{\text{T}}\rangle\\
&\vec{S}^2\,|\Phi_{\text{M1}}\rangle = |\Phi_{\text{M1}}\rangle - |\Phi_{\text{M2}}\rangle, \quad S_z\,|\Phi_{\text{M1}}\rangle = 0\\
&\vec{S}^2\,|\Phi_{\text{M2}}\rangle = |\Phi_{\text{M2}}\rangle - |\Phi_{\text{M1}}\rangle, \quad S_z\,|\Phi_{\text{M2}}\rangle = 0
\end{aligned} \tag{5}$$

The above equations show that $\Phi_{\text{M1,2}}$ are not eigenvectors of the total spin operator, but rather a mixture of singlet and $m_z = 0$ triplet-states with $\langle\Phi_{\text{M1,2}}|\vec{S}^2|\Phi_{\text{M1,2}}\rangle = 1$. Although not being eigenfunctions of the actual many-body Hamiltonian, such mixed-states appear as variational extrema in Δ-SCF calculations since approximate exchange-correlation functionals depend on m_z rather than on $\vec{S}^2$. Therefore, determining the energy of the singlet excited state requires spin-purification [56–58], whereby the energy of the singlet state is approximated through

$$E_{\text{S}} = 2\,E_{\text{M}} - E_{\text{T}}. \tag{6}$$

In this equation, E_{S} is the energy of the singlet state, E_{T} is the energy of the triplet state calculated from the density corresponding to Φ_{T} and E_{M} is the energy corresponding to either of Φ_{M1} or Φ_{M2} (note that they have the same energy, since the external potential is spin-independent). A brief derivation of Eq. (6) is provided in the Appendix.

A commonly used approach for the calculation of the singlet excited state consists in performing the Δ-SCF calculation with the spin unpolarized (NSP) exchange-correlation functional [59–62]. This type of calculation has shown to yield good agreement with experimental excitation energies. In the next section, we use and compare both the spin-purified approximation (SPA) and the NSP method for singlet energies. (In the Appendix, we provide a brief discussion of the validity of both approaches.)

As a consequence of the variational principle, the Δ-SCF calculation yields the lowest excited-state energy compatible with the imposed symmetry of the Slater determinant that was constructed from the one-electron KS states. Although it is recognized that the Δ-SCF approach lacks a formal justification (at variance with TDDFT that is based on the Runge-Gross theorem), the Δ-SCF technique is widely used in the literature and has been quite successful [11–13]. One of the formal drawbacks of the Δ-SCF method is that the exchange-correlation functional is the same for both ground and excited states (i.e., the functional form is the same with the sole difference that the excited-state density is used in place of the ground-state density). More elaborate schemes with formal justification requires the excited-state calculation to be carried out by different functionals [63, 64], by DFT methods with specific many-body

wavefunction dependence [65, 66] or by construction of ensembles with mixed ground and excited states [67–69]. In either of these cases, the needed exchange-correlation functionals are unknown, and certain approximations are necessary. For constructing ensembles, one generally relies on statistical arguments extrapolated from the interacting electron gas [70]. The success of Δ-SCF for lowest energy excitations is plausibly related to the ground-state exchange-correlation functional being sufficiently accurate to describe excited-states in some systems.

C. Hubbard model based functionals

Typically, conventional approximate exchange-correlation functionals, such as PBE, yield a poor description of localized d states for transition metals. The DFT+U approach based on an orbital-dependent correction inspired from the Hubbard model has been widely used to obtain an accurate description of electronic localization in these cases [37–40]. More recently, the extension of DFT+U, to include inter-site interactions between atomic sites (DFT+U+V), has been quite successful, not only in systems with strong electronic localization (e.g. transition-metal oxides), but also in cases where electrons are delocalized (e.g., band insulators) [41]. The V correction has also proved to be crucial in obtaining accurate structural properties of transition-metal dioxide molecules [71], and in describing the dimerization of V atoms in VO_2 accross the high-temperature to low-temperature phase transition through a DMFT approach [72]. In Ir complexes, while the on-site interaction U helps capturing the localization of d electrons on the central Ir atom, the inter-site V is expected to improve the description of the interactions with the surrounding organic ligands.

In explicit form, the corrective functional in the DFT+U+V method is given by [41]

$$E_{UV} = \sum_{I,\sigma} \frac{U^I}{2} \mathrm{Tr}\left[\mathbf{n}^{I\,I\,\sigma}\left(\mathbf{1}-\mathbf{n}^{I\,I\,\sigma}\right)\right] - \sum_{I,J,\sigma} \frac{V^{I\,J}}{2} \mathrm{Tr}\left[\mathbf{n}^{I\,J\,\sigma}\,\mathbf{n}^{J\,I\,\sigma}\right] \quad (7)$$

where U^I and $V^{I\,J}$ are on-site and inter-site interaction parameters respectively and indices I and J denote atomic sites. In Eq. (7), the occupation matrices $\mathbf{n}^{I\,J\,\sigma}$ are computed as

$$n^{I\,J\,\sigma}_{m\,m'} = \sum_i f_i^\sigma \,\langle \phi^I_m|\psi^\sigma_i\rangle\,\langle\psi^\sigma_i|\phi^J_{m'}\rangle \quad (8)$$

where ψ_i^σ are KS states, f_i^σ are their occupations, and ϕ^I_m are atomic orbitals centered on site I. The first term in Eq. (7) that is proportional to U favors electronic localization on atomic sites, while the second term proportional to V leads to hybridization between orbitals on different sites, the ground-state configuration being eventually governed by the competition between the two opposite tendencies.

IV. RESULTS AND DISCUSSIONS

The structures of the three molecules [$Ir(ppy)_3$, FIrpic, and PQIr] have been optimized using the PBE functional, and kept fixed in all TDDFT and Δ-SCF calculations. The TDDFT calculations are performed using PBE, B3LYP, and M06 functionals.

The Δ-SCF calculations were performed using the GGA, GGA+U, and GGA+U+V functionals based upon PBE using the U and V parameters obtained from linear response [40]. The details of the linear-response calculations for each of the molecules are summarized in the following subsections. In some cases, re-optimizing the structure with forces due the U and V corrections was needed.

A. $Ir(ppy)_3$

The molecular structure of $Ir(ppy)_3$ is shown in Fig. 2. The lowest triplet and singlet energies obtained within

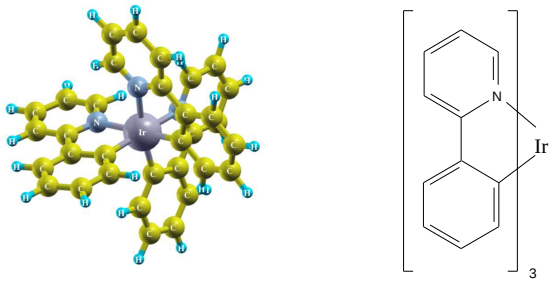

FIG. 2: (Color online) Molecular structure of $Ir(ppy)_3$ as a 3d model and a chemical formula.

TDDFT using the different semilocal and hybrid functionals are reported and compared with experiments in Table. I. Due to strong spin-orbit coupling present in

TABLE I: Lowest TDDFT triplet and singlet excited state energies compared with experiment. All values are in eV and given relative to the ground-state energy.

	Exp	GGA	B3LYP	M06
T	2.4[a]	2.09	2.55	2.55
S	2.6[b]-2.7[c]	2.16	2.75	2.79

[a] From Refs. 3, 73–82, from the highest peak in the phosphorescence spectra.
[b] From Ref. 3.
[c] From Refs. 77, 78, 82 from the second peak/shoulder in the absorption spectrum (the first absorption feature is assumed to be due to the triplet state).

these systems, it is in principle not possible to distinguish between singlet and triplet states since the actual eigenstates are mixtures of them. However, the triplet energy can be measured quite accurately in experiment from the phosphorescence spectra. The largest peak in the phosphorescence spectrum determines the energy of the triplet state, and can be determined with high accuracy [3, 73–82]. Nevertheless, in contrast to the triplet state, the experimental determination of the singlet energy is very difficult. One could in principle measure the onset of optical absorption of singlet excitons for this purpose. However, due to strong spin-orbit coupling, the optical absorption starts at much lower energies than the actual singlet energy, leaving a long tail that extends deeply into the high-wavelength region [77–83]. Another possibility is to determine the strongest peaks in the absorption spectra, which would yield much higher singlet-state energies than the lowest one. Alternatively, the LUMO-HOMO gap when the LUMO is measured by optical absorption (the so-called optical LUMO) has also been used to determine the singlet state energy [84, 85]. It is important to note that the optical LUMO contains the binding energy of the exciton unlike an inverse photoemission measurement where the exciton binding energy is eliminated [86, 87]. However, the strong spin-orbit coupling also affects such measurements since they also rely on optical absorption. Therefore, comparison of the calculated lowest singlet energy with the experimental data is not always valid, and one needs in principle to compute the absorption spectrum including spin-orbit coupling effects, which can be computationally very expensive. Relativistic effects have only recently been studied for similar dyes and was shown to result in better agreement with experiment [88]. Another uncertainty that might affect the analysis of the experimental data is whether the measurements are performed in the gas phase, in solution or for the molecule absorbed on the surface of a thin film. However, the correspondence between different types of measurements are well-known in the literature [89].

In spite of recognized difficulties in making comparison with optical measurements, we report the calculated lowest singlet excited-state energies (and trends in splittings from the triplet excited states) because they are critical for the purpose of guiding the design of OSCs with Ir dyes used as sensitizers [3].

As can be seen from Table I, the triplet excited-state energy is predicted to be within 0.1 eV from the experimental value by the hybrid functionals (B3LYP and M06), whereas it is notably underestimated by the semilocal functional (PBE). Although as already mentioned, it is very difficult to determine the lowest singlet energy experimentally, the hybrid functionals yield predictions within an error of 0.2 eV relative to the reported experimental values, whereas PBE again underestimates it. The excited-state energies reported in Table I are also in agreement with the previous results in the literature [90–93].

In order to gain further insight into computational predictions, we depict the probability density of the HOMO and the LUMO for the ground state within PBE in Fig. 3. As can be seen, the HOMO is predominantly a metal-centered state with some contribution from the ligands while the LUMO is almost entirely ligand-centered, indicating that optical excitations correlate with metal-to-ligand charge-transfer (MLCT) processes, as was previously recognized in the literature [90–95]. This charge-transfer property of the excited states also explains why the local and semilocal adiabatic approximation underestimate their TDDFT energies.

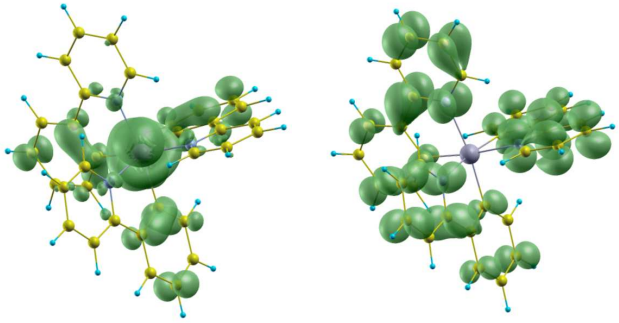

FIG. 3: (Color online) $Ir(ppy)_3$ HOMO(left) and LUMO(right) calculated using the ground-state electronic density.

The calculation of U and V parameters requires perturbing each atomic site separately for the construction of the response matrices. Instead of performing such a computationally demanding calculation including the response of all inequivalent sites, we concentrate only on the central Ir atom and its nearest neighbor C and N atoms. This approach is justified by our expectation that the electronic correlations are only important for electrons localized on the Ir atom. The atoms further away from Ir in the organic ligands (i.e., the distant C and H atoms) are taken into account in an average manner as a charge reservoir centered at the Ir site, as explained in Ref. 96. The linear response calculation yields the on-site U parameter for Ir-d (U_d) and Ir-s (U_s) states, the V parameter between Ir-d,s and neighboring C-p,s and N-p,s states [$V(\mathrm{Ir}_{d,s}, N_{p,s})$ and $V(\mathrm{Ir}_{d,s}, C_{p,s})$] and the on-site interaction parameter between Ir d and s states (V_{on}). In Table. II we report only a subset of these values, which affects the electronic structure most significantly. Further calculations, not reported here, have proven that other interaction parameters have no effect on the excited-state energies. The reported values of $V(\mathrm{Ir}_d, N_{p,s})$ and $V(\mathrm{Ir}_d, C_{p,s})$ are average values, since the distances between the three N atoms and the three C atoms to Ir atom differ slightly from one ligand to another. However, the differences are within the numerical precision of the linear-response calculations. We have also computed the inter-site interaction parameters between the Ir-d states and C-p, s states which are not nearest neighbors to the Ir atom. This calculation is performed by

TABLE II: Linear-response values of U and V parameters. We use the notation $V(\mathrm{Ir}_d, N_{p,s}) \equiv V^N_{d-p,s}$ and $V(\mathrm{Ir}_d, C_{p,s}) \equiv V^C_{d-p,s}$. All values are in eV.

U_d	V^N_{d-p}	V^C_{d-p}	V^N_{d-s}	V^C_{d-s}
7.36	1.62	1.32	2.39	2.65

isolating a chain of atoms which starts from the Ir atom and ends at a C atom in one of the ligands. The rest of the atoms in the molecule is treated as a charge reservoir, which is placed at the Ir site. As can be seen from the results shown in Figs. 4, and 5, the inter-site V parameters decay as a function of the distance from the Ir atom. This result provides a quantitative justification for the use of the nearest neighbor V parameters between Ir-N and Ir-C pairs only.

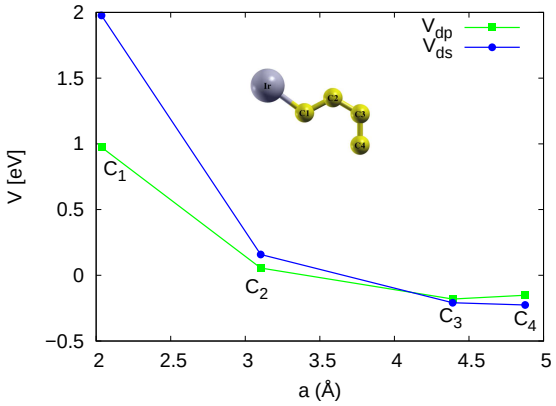

FIG. 4: Inter-site V parameters calculated for a Ir-C-C-C-C chain, as a function of distance. V_{dp} denotes the interaction parameter between Ir d and C p states, while V_{ds} denotes that between Ir d and C s states.

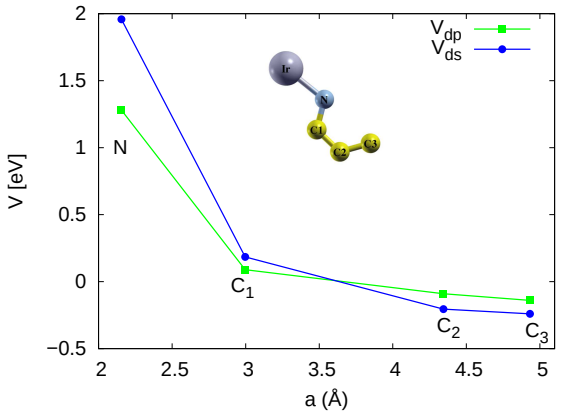

FIG. 5: Inter-site V parameters calculated for a Ir-N-C-C-C chain, as a function of distance. V_{dp} denote interaction parameter between Ir d and C,N p states, while V_{ds} denote those between Ir d and C,N s states.

The results of the Δ-SCF calculations using both the SPA singlet-state energy in Eq. (6), and its NSP counterpart are reported in Table III. Compared with the

TABLE III: Δ-SCF calculation of the lowest triplet and singlet states for $\mathrm{Ir(ppy)_3}$. All values are in eV and measured from the ground-state energy.

	GGA	U	U+V	$(\mathrm{U+V})_{\mathrm{rel}}$	Exp
T	2.32	2.27	2.41	2.44	2.4
M	2.34	2.29	2.43	2.46	–
S [NSP]	2.50	2.90	2.78	2.73	2.6-2.7
ΔE_{TS} [SPA]	0.05	0.04	0.02	0.04	–
ΔE_{TS} [NSP]	0.18	0.62	0.37	0.29	0.2-0.3

TDDFT calculations reported in Table I, the triplet energy resulting from the GGA+U and GGA+U+V calculations are slightly smaller than the triplet state energy calculated with hybrid functionals. Notice that the GGA functional within the Δ-SCF approach yields results closer to experiments than TDDFT(PBE). This is due to the ability of Δ-SCF to partially rectify charge-transfer errors. Although the energy of the triplet-state was obtained accurately, when the singlet energy is evaluated through the spin-purification formula of Eq. (6), the Δ-SCF singlet-triplet splitting is almost vanishing. On the other hand, the NSP calculation of the singlet state (S) yields results in better agreement with experiment and TDDFT. In quantitative terms within NSP, GGA+U overestimates the singlet energy by 0.3 eV, whereas GGA+U+V improves the agreement to an accuracy of approximately 0.2 eV. This improvement results from the inclusion of inter-site interactions through V, which corrects the overlocalization resulting from the straight use of the on-site U_d. In addition, when the molecular structure is re-optimized with the GGA+U+V functional [i.e. with additional forces coming from the corrective terms in Eq. (7)] , the triplet-state almost matches with the experimental value, while the singlet energy is overestimated by only 0.1 eV. Although both TDDFT and the Hubbard-corrected functionals yield results that are close to experiments, the experimental values themselves have an accuracy close to 0.2 eV [85]. Errors in the singlet energies are in principle much larger due to problems inherent to their experimental determination, as discussed above.

B. FIrpic

The molecular structure of FIrpic is shown in Fig. 6. The lowest triplet and singlet excited-state energies calculated with TDDFT using PBE, B3LYP, and M06 functionals are also compared to experimental data in Table IV. A salient feature in this comparison is the fact that the PBE functional underestimates the energies of both excited states similarly to $\mathrm{Ir(ppy)_3}$ (cf. Table I). Instead, hybrid B3LYP and M06 show a significant im-

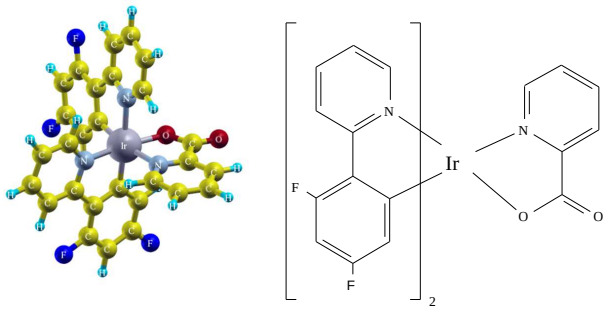

FIG. 6: (Color online) Molecular structure of FIrpic as a 3d model and a chemical formula.

TABLE IV: Lowest triplet and singlet excited-state energies obtained with TDDFT and from experiments for FIrpic. All values are in eV and measured from the ground-state energy.

	Exp	GGA	B3LYP	M06
T	2.6[a]	2.14	2.67	2.66
S	3.3[b]-2.9[c]	2.24	2.94	3.00

[a]From Refs. 2, 97–102 from the highest peak in the phosphorescence spectrum.
[b]From Ref. 97, from the second peak in the absorption spectrum.
[b]From Ref. 102, from the onset of optical absorption.

provement, and yield a triplet energy very close to experimental value. Despite the difficulties discussed in the previous section, the hybrid functionals are always within the experimental uncertainty. Therefore, we argue that they are fairly accurate.

To further explore the properties of the excited states, the HOMO and the LUMO densities in the ground state of FIrpic, are plotted in Fig. 7 within PBE. Similarly to

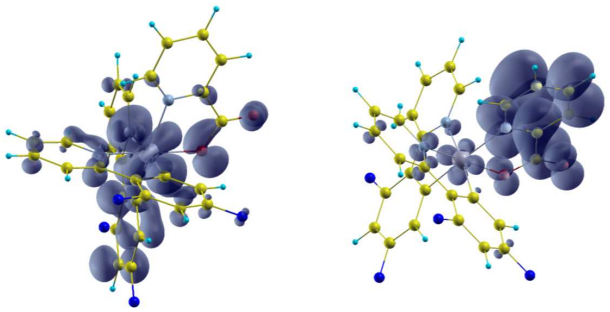

FIG. 7: (Color online) FIrpic HOMO(left) and LUMO(right) calculated using the ground-state electronic density.

$Ir(ppy)_3$, the HOMO is mostly located on Ir with considerable contribution from the ligands, whereas the LUMO is almost entirely ligand-centered on the attached chromophores [predominantly the picolinate (pic) ligand], with some contribution coming from the metal center.

The Δ-SCF calculations were performed using the GGA, GGA+U, and GGA+U+V functionals. The U and V interaction parameters were calculated using the approach described in subsection IV A. We have also checked the validity of this approach by isolating several chains containing Ir, C, N and O atoms and computing V between pairs that are not nearest neighbors. We verified that the interaction parameters between the Ir and its nearest neighbor atoms are important, while the interaction parameters between Ir and more distant shells of neighbors vanish similarly as in Figs. 4 and 5. Due to this strong similarity of the results with $Ir(ppy)_3$, we do not report these calculations here.

The calculated U and V interaction parameters for FIrpic are reported in Table. V. We report only the parameters that affect the electronic structure of the molecule most significantly, and disregard the ones that do not contribute at all. Notice that the parameters U_d, $V(\mathrm{Ir}_d, C_p)$, and $V(\mathrm{Ir}_d, N_p)$ are very close to the ones which are calculated for $Ir(ppy)_3$ reported in Table. II.

TABLE V: Linear-response values of U and V parameters. All values are in eV.

U_d	V^N_{d-p}	V^C_{d-p}	V^O_{d-p}	V^N_{d-s}	V^C_{d-s}	V^O_{d-s}
7.17	1.69	1.29	2.0	3.06	2.56	5.77

The results of the Δ-SCF calculations using both the SPA and NSP calculations for the singlet state are reported in Table VI. As for $Ir(ppy)_3$, GGA within Δ-SCF yields excited-state energies in better agreement with experimental data compared to GGA within TDDFT. While GGA+U overestimates the triplet energy by approximately 0.2 eV, GGA+U+V lowers it by 0.2 eV, that is, within 0.1 eV of experiments. Additionally, the singlet state energies predicted by GGA+U and GGA+U+V fall within the experimental range, as was the case for TDDFT with hybrid functionals.

TABLE VI: Δ-SCF calculation of the lowest triplet and singlet states. All values are in eV and given relative to the ground-state.

	GGA	U	U+V	$(U+V)_{rel}$	Exp
T	2.46	2.79	2.56	2.52	2.6
M	2.50	N.A.[a]	2.60	2.56	–
S [NSP]	2.65	3.00	2.88	2.81	3.3-2.9
ΔE_{TS} [SPA]	0.08	N.A[a]	0.08	0.08	–
ΔE_{TS} [NSP]	0.18	0.20	0.31	0.29	0.3-0.7

[a]No convergence is achieved for these calculations.

Yet, compared to $Ir(ppy)_3$, the excited-state energies are higher in FIrpic, explaining the blue phosphorescence of FIrpic. We thus confirm a well-known experimental result that the attachment of F atoms in the ligands stabilize the HOMO level and increase the LUMO-HOMO energy gap [103, 104]. Since F is highly electronegative, it decreases the amount of charge localized on the metal center, thereby reducing the total Coulomb repulsion felt by these electrons and stabilizing the HOMO level. This

comparison with $Ir(ppy)_3$ suggests that further adjustments on the triplet emission energy can be obtained by functionalizing the (pic) ligand, since the LUMO is mainly localized on it, as can be seen from Fig. 7.

C. PQIr

The molecular structure of PQIr is shown in Fig. 8. The lowest triplet and singlet excited-state energies

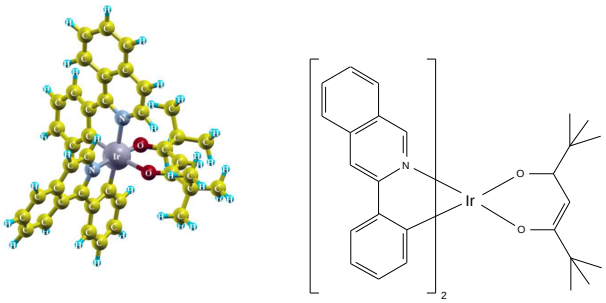

FIG. 8: (Color online) Molecular structure of PQIr as a 3d model and a chemical formula.

within TDDFT using GGA (PBE), B3LYP, and M06 are reported in Table. VII. As for the other molecules studied in this paper, TDDFT(PBE) underestimates both the triplet and the singlet energies while the hybrid functionals yield results within an error of 0.1 eV relative to experiment.

TABLE VII: Lowest triplet and singlet excited-state energies obtained with TDDFT and from experiments for PQIr. All values are in eV and measured from the ground state.

	Exp	GGA	B3LYP	M06
T	2.1[a]	1.63	2.02	2.01
S	2.3[b]	1.74	2.35	2.37

[a] From Refs. 2, 75, 105 from the highest peak in the phosphorescence spectrum.

[b] From Ref. 105–107, from the LUMO-HOMO energy difference, where the LUMO is treated as an "optical LUMO" which also contains the exciton binding energy [84, 85] (which is a singlet state).

The HOMO and the LUMO charge distributions are depicted in Fig. 9 for the ground state within PBE. Here, in accordance with the other Ir dyes, the HOMO is predominantly centered on the metal, with some contributions from the ligands. Instead, the LUMO is almost entirely ligand-centered. Notice that the tetramethyl heptanedionate (tmd) ligand only contributes (marginally) to the HOMO, and the LUMO is concentrated on the larger phenyl-quinoline (pq) ligand.

The calculated U and V parameters are reported in Table VIII. As before, we only report interaction parameters that affect the electronic structure most significantly. The validity of restricting our calculations to

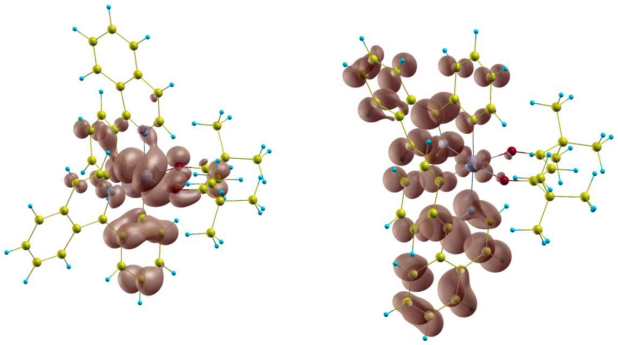

FIG. 9: (Color online) PQIr HOMO(left) and LUMO(right) calculated using the ground-state electronic density.

TABLE VIII: Linear-response values of U and V parameters. All values are in eV.

U_d	V^N_{d-p}	V^C_{d-p}	V^O_{d-p}	V^N_{d-s}	V^C_{d-s}	V^O_{d-s}
7.26	1.71	1.39	1.79	2.66	4.43	5.40

Ir and its nearest neighbors was also verified for PQIr, by computing U and V parameters between the atoms along several "chains" from the central Ir towards the external ligands and showing that only nearest neighbor interactions are important. The calculated U_d and V for Ir-N, Ir-C, and Ir-O pairs between d and p states are also very close to the ones computed previously for the other two molecules. This finding suggests that these parameters could be considered to be universal and used for future studies without recomputing them for each molecule (provided that the same pseudo-potential and exchange-correlation functional are used).

The results of the Δ-SCF calculations using the GGA, GGA+U, and GGA+U+V functionals are reported in Table IX. Again, GGA yields results in better accordance

TABLE IX: Δ-SCF calculation of the lowest triplet and singlet states for PQIr. All values are in eV and given relative to the ground-state.

	GGA	U	U+V	$(U+V)_{rel}$	Exp
T	1.81	2.11	1.93	1.90	2.1
M	1.79	2.18	1.98	1.95	–
S [NSP]	2.01	2.34	2.23	2.18	2.3
ΔE_{TS} [SPA]	0.06	0.14	0.10	0.10	–
ΔE_{TS} [NSP]	0.19	0.23	0.30	0.28	0.2

with experiment within Δ-SCF than within TDDFT. The best agreement with the reported experimental values in Table VII are obtained with GGA+U, using the NSP calculation of the singlet state. This might seem to contradict the results for $Ir(ppy)_3$ and FIrpic, where the best agreement was found with the inclusion of V. However, it should be noted that the experimental results have an accuracy of approximately 0.2 eV [85]. Thus,

GGA+U+V results are within this range of this accuracy.

The excited-state energies of PQIr are smaller than those of $Ir(ppy)_3$ and FIrpic, which accounts for its red phosphorescent emission. This is due to the stabilization of the LUMO level resulting from the larger size of the (pq) ligand where it is mostly centered on (see Fig. 9). In fact the (pq) ligand has an additional benzene ring compared to $Ir(ppy)_3$. A larger ligand structure can be expected to lower the electron-electron interactions and reduce the electronic kinetic energy through a more pronounced delocalization, hence the stabilization of the electronic states it hosts (the LUMO level in this case) [108].

D. Comparison of TDDFT and Δ-SCF

As discussed briefly in subsection III A, TDDFT yields inaccurate energies for charge-transfer excitations, specifically if used with local and semilocal functionals, like GGA(PBE). As we have shown in Figs. 3, 7 and 9, the excited states of the Ir dyes studied in this work are of MLCT type. The MLCT character of the excited-states explains why GGA underestimates the excited-state energies, whereas the hybrid functionals provide better agreement with the experimental measurements, which are reported in Tables I, IV, and VII. Instead, PBE within the Δ-SCF approach using the NSP representation of the singlet state proves to be more accurate than TDDFT, as can be seen from Tables III, VI, and IX. Indeed, the fact that Δ-SCF could perform better than TDDFT for charge-transfer and Rydberg excitations is already known from the literature [11–13, 54, 55]. TDDFT relies on KS energies determined from the ground-state configuration, and in the case of charge-transfer excitations, the effect of unoccupied orbitals are not accurately taken into account by semilocal functionals since the off-diagonal block matrices ($\mathbf{M}$) nearly vanishes in Eq. (1). This is due to the fact that the exchange-correlation potential decays exponentially with distance r, rather than as $O(r^{-1})$. Instead, Δ-SCF takes into account the orbital relaxation of ground-state KS states, since those are reconstructed at each iteration from an excited-state density [Eq. (4)]. If expanded using the basis of unrelaxed orbitals, the relaxed orbitals include components from the unoccupied manifolds that are not properly taken into account by TDDFT used with (semi)local functionals. As a result, the effect of the unoccupied manifold (with respect to ground-state KS orbitals) is partially included in Δ-SCF. Along the same lines, Ref. 54 has shown that the long-range behavior of the Δ-SCF energies can be more accurate than TDDFT.

Comparing Tables I, IV, VII with Tables III, VI, IX one can observe that hybrid functionals within TDDFT performs similarly to Δ-SCF calculations with Hubbard corrections. This shows that both methods can be used interchangeably. In explicit terms, one can use Δ-SCF with hybrid functionals or TDDFT with Hubbard U and V corrections, where the latter approach would allow for significantly less computational effort for large systems than hybrid functionals. One other notable advantage of the Hubbard corrected functionals is that the U and V parameters directly control the amount of electronic localization on the Ir atom and the hybridization between Ir and the surrounding ligands. This knowledge could provide a functionalization strategy for tuning the excited-state energy levels, as discussed briefly in the next subsection.

E. Effects of U and V

In order to investigate the effects of the Hubbard corrections more systematically, we provide a simple model of the system, based on two atomic states, one centered on the metal and the other centered on the ligand, as shown schematically in Fig. 10. In this simplified picture, we assume that the HOMO levels ψ_N^σ have large overlap with the metal orbital ϕ^M, and a small overlap with the ligand orbital ϕ^L. Instead, the LUMO levels have large overlap with the ligand orbital ϕ^L but a small overlap with the metal orbital ϕ^M. The contribution of the Hubbard corrective energy in Eq. (7) in the case of two atomic orbitals ϕ^M and ϕ^L (which are assumed non-degenerate) becomes

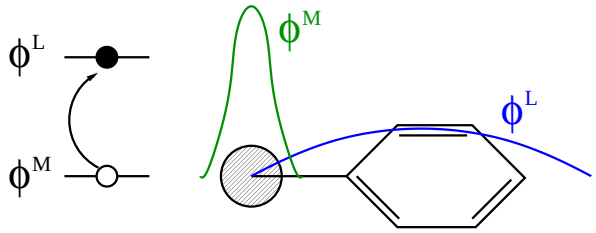

FIG. 10: A simple description of the MLCT character of the excited states in the Ir complexes.

$$E_{\rm UV} = \frac{U_M}{2}\sum_\sigma n^{M\sigma}\left(1-n^{M\sigma}\right) - V^{ML}\sum_\sigma n^{ML\sigma}\,n^{LM\sigma} \tag{9}$$

where

$$\begin{aligned} n^{M\sigma} &= \sum_i f_i^\sigma\,|\langle\phi^M|\psi_i^\sigma\rangle|^2 \\ n^{ML\sigma} &= \sum_i f_i^\sigma\,\langle\phi^M|\psi_i^\sigma\rangle\langle\psi_i^\sigma|\phi^L\rangle \end{aligned} \tag{10}$$

In the above equations, the occupation numbers f_i^σ are either 1 or 0. We also assume that the occupation matrices are symmetric, i.e., $n^{ML\sigma} = n^{LM\sigma}$. We can construct the occupation matrices n^M, n^L, n^{ML} by ignoring the orbital relaxation and using the levels schematically

represented in Fig. 1. For example, in the triplet state, the occupation matrices are given by

$$n_{\rm T}^{M\uparrow} = n_{\rm G}^{M\uparrow} + \Delta\, n_{N+1}^{\uparrow} \;\;,\;\; n_{\rm T}^{M\downarrow} = n_{\rm G}^{M\downarrow} - \Delta\, n_{N}^{\downarrow}$$
$$n_{\rm T}^{ML\uparrow} = n_{\rm G}^{ML\uparrow} + \Delta\, n_{N+1}^{ML\uparrow} \;\;,\;\; n_{\rm T}^{ML\downarrow} = n_{\rm G}^{ML\downarrow} - \Delta\, n_{N}^{ML\downarrow} \tag{11}$$

where

$$\begin{aligned} \Delta n_{N+1}^{\uparrow} &\equiv |\langle\phi^{M}|\psi_{N+1}^{\uparrow}\rangle|^2 \;\;,\;\; \Delta n_{N}^{\downarrow} \equiv |\langle\phi^{M}|\psi_{N}^{\downarrow}\rangle|^2 \\ \Delta n_{N+1}^{ML\uparrow} &\equiv \langle\phi^{M}|\psi_{N+1}^{\uparrow}\rangle\,\langle\psi_{N+1}^{\uparrow}|\phi^{L}\rangle \\ \Delta n_{N}^{ML\downarrow} &\equiv \langle\phi^{M}|\psi_{N}^{\downarrow}\rangle\,\langle\psi_{N}^{\downarrow}|\phi^{L}\rangle \end{aligned} \tag{12}$$

Since ψ_N^σ is dominantly metal-centered, while ψ_{N+1}^σ is ligand centered, $\Delta n_{N+1}^{\uparrow} \ll 1$ is satisfied, whereas $\Delta n_{N+1}^{ML\uparrow}$ and $\Delta n_{N}^{ML\downarrow}$ can in principle be larger, but still considerably smaller than 1. Instead, $\Delta n_N^{\downarrow}$ is of the order of 1. In Eq.(11), the subscripts G and T refers to occupation matrices evaluated from the ground-state and triplet-state, respectively. We can calculate the contribution to the excited-state energies from Hubbard terms as $E_{UV}^{\rm T} - E_{UV}^{\rm G}$ by using Eqs. (9)-(12). The contribution coming from the on-site interactions [i.e., the first term in Eq. (9)] is given by

$$\begin{aligned} E_U^{\rm T} - E_U^{\rm G} \equiv \omega_{\rm T}^{U} \;&=\; -\frac{U_M}{2}\,\Delta n_N^{\downarrow}\left(1 + \Delta n_N^{\downarrow} - n_{\rm G}^{M}\right) \\ &+\; \frac{U_M}{2}\,\Delta n_{N+1}^{\uparrow}\left(1 - n_{\rm G}^{M}\right) + {\rm O}\left(\Delta n_{N+1}^{2}\right) \end{aligned} \tag{13}$$

where we have ignored quadratic terms in $\Delta n_{N+1}^{\uparrow}$ and used the fact that $n_{\rm G}^{\uparrow} = n_{\rm G}^{\downarrow} = \frac{1}{2}\, n_{\rm G}$. The first term in Eq. (13) is negative, since $1 + \Delta_N^{\downarrow} > 1$, while $n_{\rm G}^{M} < 1$. Instead, the second term is positive. Therefore, Eq. (13) shows that the excited-state energy decreases with increasing U_M, which is expected since larger U_M destabilizes the HOMO level by adding larger penalty when it is doubly occupied in the ground-state. However, for cases where there is considerable metal and ligand overlap, the second term in Eq. (13) can reverse this effect through a larger $\Delta n_{N+1}^{\uparrow}$. To test this prediction, we have plotted in Fig. 11 the energies of the triplet and singlet state (obtained from a NSP calculation) as a function of U_d for Ir(ppy)$_3$. As can be seen from Fig. 11, the triplet energy increases for $U_M \leq 5\,$eV, but decreases for larger values of U_M. This decreasing behavior is correctly predicted by Eq. (13). Instead, the increase in the triplet energy for $U_M \leq 5\,$eV is probably a result of important modifications in the KS states due to orbital relaxation which is implicitly ignored in deriving Eq. (13). For the case of the molecules studied in this work, $U_d \gtrsim 7\,$eV. Therefore an increasing U_d would decrease the triplet energy, mainly due to the destabilization of the HOMO level. The singlet state is a result of a NSP calculation, and its behavior as a function of U_M is thus difficult to assess

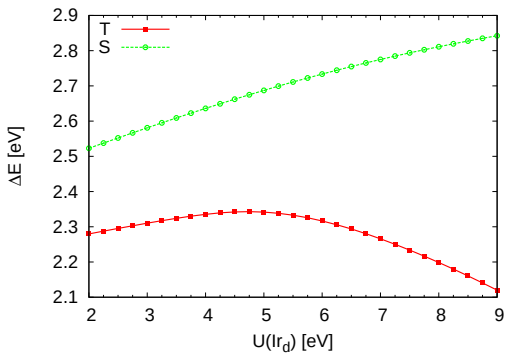

FIG. 11: Triplet and singlet energies computed as a function of on-site U on Ir d states. No inter-site V is included.

since in principle it corresponds to an ensemble which contains an arbitrary combination of possible different Slater determinants, as discussed in the Appendix.

The contribution from the inter-site interaction terms in Eq. (9) to the excited-state energy can be calculated similarly. Doing so, we obtain

$$\begin{aligned} E_V^{\rm T} - E_V^{\rm G} \equiv \omega_{\rm T}^{V} \;&=\; -V^{ML}\, n_{\rm G}^{ML}\left(\Delta n_{N+1}^{LM\uparrow} - \Delta n_{N}^{ML\downarrow}\right) \\ &+ {\rm O}\left(\Delta^2\right) \end{aligned} \tag{14}$$

where we have ignored the quadratic terms in Δn_N and Δn_{N+1}. Note that the term given in Eq. (14) could be either positive or negative depending on the relative magnitude of the projections $\Delta n_{N+1}^{LM\uparrow}$ and $\Delta n_{N}^{ML\downarrow}$. For example, in the case of a strong metal-LUMO overlap but a smaller ligand-HOMO overlap, V decreases the triplet energy. Instead, in the opposite case where the ligand-HOMO overlap is larger than the metal-LUMO overlap, V increases the triplet energy. In order to validate these predictions, we have plotted the triplet and singlet (from NSP calculation) state energies as a function of the V between Ir d and C and N p and s states in Fig. 12. In these calculations, we have fixed the value of U_d to the calculated value of 7.36 eV and used the same V between all the Ir-C and Ir-N pair interactions. As can be seen from Fig. 12, the triplet energy increases for $V \leq 1.5\,$eV and decreases for $V \geq 1.5\,$eV, reflecting both type of behaviors shown in Eq. (14). In this case, the orbital relaxation effects, which are ignored in obtaining Eq. (14) are more critical since they affect the overlap of the HOMO and LUMO levels (ψ_N^σ, ψ_{N+1}^σ) with the metal-and-ligand-centered states. This contribution can very easily invert the behavior of the triplet energy as a function of V. In summary, Figs. 11 and 12 show that the excited-state energies critically depend on the U and V values, which highlights the sensitivity of these energies to small chemical changes. In fact, as discussed in previous sections, a change in the chemical composition of the ligand groups can result in modifications to the electronic structure of these molecules analogous to those obtained by varying U and V. This conclusion was also obtained in a different

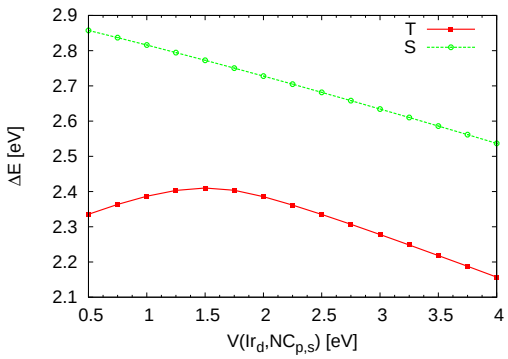

FIG. 12: Triplet and singlet energies computed as a function of inter-site V between Ir d and C,N s, p states. $U = 7.36\,\text{eV}$ fixed at the computed value.

way by using model Hamiltonians in Refs. 109 and 110. In fact, the results presented in Tables II, V and VIII can be used as effective parameters in a model-Hamiltonian study for these systems.

Summarizing, for the three molecules that we have studied in this work, two distinct behaviors are observed. For $Ir(ppy)_3$, the effect of the U and V corrections is mainly to tune the HOMO level. The addition of U decreases the excited-state energies (see Table III) due to the destabilization of the HOMO level, which is dominantly metal-centered. This destabilization arises from an increased Coulomb repulsion between the two electrons occupying the HOMO level. Instead, with the addition of V, the HOMO level is stabilized, increasing the excitation energies. This is due to the increased hybridization between Ir and neighboring atoms, which depletes the Ir d states, lowering the Coulomb repulsion on them. In contrast, for FIrpic and PQIr, the addition of U and V affects mainly the LUMO level. Including U increases the excited-state energies (see Tables VI and IX) due to the destabilization of the LUMO level. This trend can be ascribed to the fact that the LUMO level contains a non-negligible contribution from the metal, as compared to $Ir(ppy)_3$ (compare Fig. 3 with Figs. 7 and 9). Instead, the addition of V stabilizes the LUMO by lowering the fraction of electrons localized on the metal-center. In a nutshell, this study suggests that the substitution of atoms close to the Ir center can be as effective in the functionalization of the complex as the well known addition of F or other electronegative species to the external part of the ligands or modifications of their structure.

V. CONCLUSION

In this work, we have studied the electronic structure of the lowest triplet and singlet excited-states of three representative iridium dyes. The calculation of the excited-state energies were performed using TDDFT with hybrid functionals and Δ-SCF with Hubbard corrections namely, GGA+U and GGA+U+V. The results obtained in both approaches are in good agreement with experiment. The Hubbard corrections U and V were computed from ab-initio calculations and provide a measure for localization and hybridization of Ir d states with neighboring organic ligands in the ground and excited-states. This knowledge is used to infer possible strategies for tuning the excited-state energies of the studied molecules. The gained insight underscores the interest of Hubbard corrections in unveiling the electronic origin of dye phosphorescence. In addition, we have also investigated the validity of the spin purification (SPA) and the nonspin-polarized (NSP) calculations for the computation of the singlet excited-state energy. We found that the SPA approach (based on the construction of a state with mixed spin symmetry) clearly underestimates the experimental singlet energies. Instead, the NSP calculation yields much more accurate results. While the failure of the spin purification formula can be understood from the inadequacies of the conventional exchange-correlation functionals, the remarkable success of the NSP approach in capturing the singlet remains a relevant open question.

The present work can be considered as the starting point of two main research directions involving methodological developments on one side and the design and optimization of better molecular complexes, on the other. From a methodological point of view this study highlights the necessity to improve functionals that can distinguish between different $\langle \vec{S}^2 \rangle$ configurations (with the inclusion of spin-orbit interactions). On the application side this work establishes DFT+U+V as a valid computational tool (thanks to its ability to capture the charge-transfer character of excited states) to efficiently screen useful modification to the ligand structure of the considered molecules that could improve their performance. Furthermore, the dependence of the energy splittings on the values of U and, more importantly, of V, suggests that the choice of the chemical species directly bonded with the Ir center and of the structure of the ligands in its coordination shell may represent another valuable route to functionalization that can be explored in addition to the modification of their most external part.

Acknowledgments

We thank Minnesota Supercomputing Institute (MSI) for providing the computational resources used in this work. This work is supported by the Seed grant provided by Materials Research Science and Engineering Center (MRSEC) of the University of Minnesota. M.C also acknowledges partial support from NSF EAR 0810272 and from the NSF CAREER award DMR 1151738.

Appendix A: Comparison of spin-purification and NSP calculations

In section IV, we have shown that the Δ-SCF energy for the mixed spin states $\Phi_{\mathrm{M1,2}}$ used in the SPA formula Eq. (6) yields much lower singlet state energies than the experimental results. Instead, the NSP Δ-SCF calculation yields results within the experimental accuracy of 0.2 eV. In this Appendix, we provide some insight into this finding.

Approximate exchange-correlation functionals depend only on the spin component m_z, and cannot distinguish between $m_z = 0$ triplet and singlet states. Moreover, with approximate exchange-correlation functionals and integer occupations, only configurations that can be represented by a single Slater determinant are obtained as stationary densities in Δ-SCF calculations. Instead, the $m_z = 0$ triplet and singlet states correspond to multi-Slater-determinant configurations, represented by the following density matrices (excluding orbital relaxation effects)

$$\begin{aligned}\hat{D}_{1,0} = \frac{1}{2}\Big[&|\Phi_{\mathrm{M1}}\rangle\langle\Phi_{\mathrm{M1}}| - |\Phi_{\mathrm{M1}}\rangle\langle\Phi_{\mathrm{M2}}| \\ &-|\Phi_{\mathrm{M2}}\rangle\langle\Phi_{\mathrm{M1}}| + |\Phi_{\mathrm{M2}}\rangle\langle\Phi_{\mathrm{M2}}|\Big] \quad \text{(A1)}\\ \hat{D}_{0,0} = \frac{1}{2}\Big[&|\Phi_{\mathrm{M1}}\rangle\langle\Phi_{\mathrm{M1}}| + |\Phi_{\mathrm{M1}}\rangle\langle\Phi_{\mathrm{M2}}| \\ &+|\Phi_{\mathrm{M2}}\rangle\langle\Phi_{\mathrm{M1}}| + |\Phi_{\mathrm{M2}}\rangle\langle\Phi_{\mathrm{M2}}|\Big] \quad \text{(A2)}\end{aligned}$$

where $\hat{D}_{1,0}$ corresponds to the density matrix of the $m_z = 0$ triplet, while $\hat{D}_{0,0}$ corresponds to the density matrix of the singlet state. Eqs. (A1) and (A2) can easily be verified by evaluating the expectation value of the total spin square operator, and making use of Eq. (5) as

$$\begin{aligned}\langle\vec{S}^2\rangle_{1,0} &= \mathrm{Tr}\left[\hat{D}_{1,0}\,\vec{S}^2\right] = 2\\ \langle\vec{S}^2\rangle_{0,0} &= \mathrm{Tr}\left[\hat{D}_{0,0}\,\vec{S}^2\right] = 0. \quad \text{(A3)}\end{aligned}$$

Instead, the single-particle density is the same for both states, and is given by

$$\begin{aligned}n(\mathbf{r}) &= \mathrm{Tr}\left[\hat{D}\hat{n}(\mathbf{r})\right]\\ &= \frac{1}{2}\langle\Phi_{\mathrm{M1}}|\hat{n}(\mathbf{r})|\Phi_{\mathrm{M1}}\rangle + \frac{1}{2}\langle\Phi_{\mathrm{M2}}|\hat{n}(\mathbf{r})|\Phi_{\mathrm{M2}}\rangle. \quad \text{(A4)}\end{aligned}$$

Notice that the off-diagonal terms $\langle\Phi_{\mathrm{M1}}|\hat{n}(\mathbf{r})|\Phi_{\mathrm{M2}}\rangle$ vanish when orbital relaxation effects are ignored (i.e. the states $\Phi_{\mathrm{M1,2}}$ are fixed). With the inclusion of orbital relaxation effects, the densities of $m_z = 0$ triplet and singlet states would be different. However, realization of this difference requires an ensemble dependent functional [67–70]. More specifically, the ensemble exchange-correlation functional should depend on the weights of the Slater determinants appearing in the density matrices Eq. (A1) and (A2). In fact, any density matrix of the form $q\,\hat{D}_{1,0} + (1-q)\,\hat{D}_{0,0}$ with $q \leq 1$, results precisely in the same one particle density Eq. (A4), with $\langle\vec{S}^2\rangle = 2\,q$. Without a functional that depends on the ensemble weights (i.e., q in this case) or a functional that can distinguish between states with different $\vec{S}^2$, it is not possible to know which ensemble $n(\mathbf{r})$ corresponds to. In the absence of such a functional, one relies on the calculation of the expectation value of the many-body Hamiltonian operator using DFT with standard exchange-correlation functionals, which are given by

$$\begin{aligned}E_{1,0} &= \mathrm{Tr}\left[\hat{D}_{1,0}\,\mathcal{H}\right]\\ &= \frac{1}{2}\langle\Phi_{\mathrm{M1}}|\mathcal{H}|\Phi_{\mathrm{M1}}\rangle + \frac{1}{2}\langle\Phi_{\mathrm{M2}}|\mathcal{H}|\Phi_{\mathrm{M2}}\rangle\\ &\quad -\frac{1}{2}\left[\langle\Phi_{\mathrm{M1}}|\mathcal{H}|\Phi_{\mathrm{M2}}\rangle + \text{c.c.}\right]\\ E_{0,0} &= \mathrm{Tr}\left[\hat{D}_{0,0}\,\mathcal{H}\right]\\ &= \frac{1}{2}\langle\Phi_{\mathrm{M1}}|\mathcal{H}|\Phi_{\mathrm{M1}}\rangle + \frac{1}{2}\langle\Phi_{\mathrm{M2}}|\mathcal{H}|\Phi_{\mathrm{M2}}\rangle\\ &\quad +\frac{1}{2}\left[\langle\Phi_{\mathrm{M1}}|\mathcal{H}|\Phi_{\mathrm{M2}}\rangle + \text{c.c.}\right]\end{aligned} \quad \text{(A5)}$$

Assuming that the expectation value of the many-body Hamiltonian can approximately be given by Δ-SCF calculations, one can identify the mixed-state energy as the variational extrema given by

$$\langle\Phi_{\mathrm{M1,2}}|\mathcal{H}|\Phi_{\mathrm{M1,2}}\rangle = E_{\mathrm{M}}. \quad \text{(A6)}$$

Since the Hamiltonian does not contain any external magnetic fields, $m_z = 1$ and $m_z = 0$ triplet states should have the same energy, which requires

$$\langle\Phi_{\mathrm{T}}|\mathcal{H}|\Phi_{\mathrm{T}}\rangle = E_{\mathrm{T}} = E_{1,0} \quad \text{(A7)}$$

Then, adding the two equations in Eq. (A5) to cancel the off-diagonal terms, and using Eqs. (A7) and (A6), one obtains the spin purification formula given in Eq. (6): $E_{\mathrm{T}} + E_{\mathrm{S}} = 2E_{\mathrm{M}}$ (with $E_{\mathrm{S}} = E_{0,0}$) [56–58].

The reason why the Δ-SCF energy of the mixed-state (E_{M}), used in spin-purification formula Eq. (6), underestimates the experimental singlet energies can be understood, in part, by carefully examining the assumptions that were made in the discussion above. First, the assumption in Eq. (A7) is not justified. Approximate ground-state exchange-correlation functionals can distinguish between states with different m_z, but not with different $\langle\vec{S}^2\rangle$, as discussed previously. Therefore, Eq. (A7) assumes the equality of energies of a single determinant state Φ_{T} and an ensemble $\hat{D}_{1,0}$, which have different m_z. In other words, $\langle\Phi_{\mathrm{T}}|\mathcal{H}|\Phi_{\mathrm{T}}\rangle$ is not a good estimate of E_{T}. Such an identification is clearly beyond the capabilities of approximate exchange-correlation functionals. Eq. (A7) can be justified only if an appropriate ensemble exchange-correlation functional is used. Second, the spin purification formula is plagued by the negligence of

orbital relaxation effects. The ensemble density matrices of the singlet and $m_z = 0$ triplet states of Eqs. (A1) and (A2) suggests that they are equal-weight combinations of the mixed-states $\Phi_{\rm M1}$ and $\Phi_{\rm M2}$. The spin purification formula critically depends on this equivalence of the weights. However, when orbital relaxation effects are included, KS orbitals corresponding to $\Phi_{\rm M1}$ are $\Phi_{\rm M2}$ are different and, in general, the transformation between them requires an infinite expansion, including infinite set of states in the unoccupied manifolds. Thus, an actual ensemble representation of the singlet and $m_z = 0$ triplet-states should contain contribution from such an infinite expansion (e.g. on unrelaxed KS orbitals). Namely, the ensembles must include a linear combination of many excited-state determinants with orbitals ψ_a^σ occupied where $a > N + 1$. Such an approach is not viable, since constructing a functional that depends on the weights of each excited Slater determinant is not easy. At this point we would like to stress that ensemble DFT of Refs. 67–70, does not suffer from such problems, provided that an ensemble dependent exchange-correlation functional exists. In this case, the energy of each state in the ensemble is uniquely determined by the Hohenberg-Kohn theorem for ensembles [67].

The success of the NSP Δ-SCF calculation is more difficult to understand. The NSP state used for the Δ-SCF calculation, $\Phi_{\rm NSP}$, exactly corresponds to a transition state with orbitals ψ_N and ψ_{N+1} occupied by half spin-up and half-spin down electrons, as shown schematically in Fig. 13. It is well-known that the single particle density of a transition state [111] is equivalent to an ensemble density [68, 112]. Indeed, the corresponding single particle density obtained from $\Phi_{\rm NSP}$ is given by

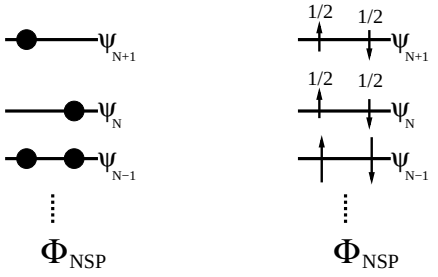

FIG. 13: $\Phi_{\rm NSP}$ schematically represented both by spin-unpolarized orbitals and an equivalent transition state.

$$n_{\rm NSP}(\mathbf{r}) = \sum_{i=1,\sigma}^{N-1} |\psi_i^\sigma(\mathbf{r})|^2 + \frac{1}{2}\Big[|\psi_N^\uparrow(\mathbf{r})|^2 + |\psi_N^\downarrow(\mathbf{r})|^2 + |\psi_{N+1}^\uparrow(\mathbf{r})|^2 + |\psi_{N+1}^\downarrow(\mathbf{r})|^2\Big] \tag{A8}$$

When orbital relaxation effects are taken into account, Eq. (A8) still holds, since spin-up and spin-down orbitals are always equivalent due to magnetization density being identically zero (so that the exchange-correlation functional is spin non-polarized). Moreover, Eq. (A8) is identical to Eq. (A4), i.e., the densities of the $m_z = 0$ triplet and singlet states, when orbital relaxation effects are ignored. Since $n_{\rm NSP}(\mathbf{r})$ already provides a direct calculation of an ensemble density, unlike the spin-purification formula which relies on a spurious mixed-state $\Phi_{\rm M1,2}$, it can be expected that $n_{\rm NSP}(\mathbf{r})$ could provide more accurate results. However, $n_{\rm NSP}(\mathbf{r})$ could in principle be a linear combination of other types of excited single determinant states. For instance, consider a doubly excited state Φ_*, which is schematically represented in Fig. 14. The single-particle density $n_{\rm NSP}(\mathbf{r})$ can be obtained from

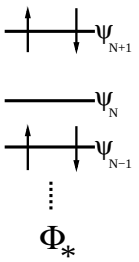

FIG. 14: Doubly excited-state that can participate in $n_{\rm NSP}(\mathbf{r})$.

the following ensemble density matrix

$$\hat{D}_* = \frac{1}{2}\,|\Phi_{\rm G}\rangle\langle\Phi_{\rm G}| + \frac{1}{2}\,|\Phi_*\rangle\langle\Phi_*| \tag{A9}$$

More generally, $n_{\rm NSP}(\mathbf{r})$ can be obtained from an ensemble of the form

$$\hat{D} = \frac{1-q}{2}\,\hat{D}_{1,0} + \frac{q}{2}\,\hat{D}_{0,0} + \frac{1}{4}\,|\Phi_{\rm G}\rangle\langle\Phi_{\rm G}| + \frac{1}{4}\,|\Phi_*\rangle\langle\Phi_*| \tag{A10}$$

where $q \leq 1$. The reason why $n_{\rm NSP}(\mathbf{r})$ results in better singlet energies could be related to the fact that it corresponds to an ensemble Eq. (A10), rather than a single determinant description of mixed spin states. Moreover, it is the only variational minimum that one can obtain using approximate ground-state exchange-correlation functionals which has this property. Due to the variational principle, one could expect that contributions from Φ_* to be suppressed, since it is not the lowest energy configuration with vanishing spin polarization. However, it is not possible to have control over the ensemble weights appearing in Eq. (A10) with approximate ground-state exchange-correlation functionals. Indeed, hints of this problem can be seen in Fig. 11 where the singlet energy was found to increase with U_d almost linearly. One expects that larger U_d to destabilize the HOMO level, leading to a decreasing singlet energy. Due to the same reason, the ground-state energy should increase with U_d. Thus, an increasing singlet energy in Fig. 11 is an indication that the NSP state contains ground-state contributions. The arbitrariness in

the ensembles that represent $n_{\mathrm{NSP}}(\mathbf{r})$, limits the understanding of the NSP Δ-SCF calculation. Therefore, the use of $n_{\mathrm{NSP}}(\mathbf{r})$ is only partially justified, and mostly motivated by its empirical success presented in section IV and previous studies in the literature [59–61].

[1] M. Baldo, D. O'brien, Y. You, A. Shoustikov, S. Sibley, M. Thompson, and S. Forrest, Nature **395**, 151 (1998).
[2] L. Xiao, Z. Chen, B. Qu, J. Luo, S. Kong, Q. Gong, and J. Kido, Adv. Mater. **23**, 926 (2011).
[3] W. A. Luhman and R. J. Holmes, Appl. Phys. Lett **94**, 3 (2009).
[4] Y. Shao and Y. Yang, Adv. Mater. **17**, 2841 (2005).
[5] L. Hedin, Phys. Rev **139**, A796 (1965).
[6] G. Onida, L. Reining, and A. Rubio, Rev. Mod. Phys. **74**, 601 (2002).
[7] E. Runge and E. Gross, Phys. Rev. Lett **52**, 997 (1984).
[8] M. Petersilka, U. Gossmann, and E. Gross, Phys. Rev. Lett **76**, 1212 (1996).
[9] T. Grabo, M. Petersilka, and E. Gross, J. Mol. Struct. THEOCHEM **501**, 353 (2000).
[10] T. Ziegler, A. Rauk, and E. Baerends, Theor. Chem. Acc. **43**, 261 (1977).
[11] M. Casida, F. Gutierrez, J. Guan, F. Gadea, D. Salahub, and J. Daudey, J. Chem. Phys. **113**, 7062 (2000).
[12] C. Cheng, Q. Wu, and T. Van Voorhis, J. Chem. Phys. **129**, 124112 (2008).
[13] T. Kowalczyk, S. Yost, and T. Voorhis, J. Chem. Phys. **134**, 054128 (2011).
[14] D. Tozer, J. Chem. Phys **119**, 12697 (2003).
[15] A. Dreuw, J. Weisman, and M. Head-Gordon, J. Chem. Phys. **119**, 2943 (2003).
[16] M. Casida, C. Jamorski, K. Casida, and D. Salahub, J. Chem. Phys. **108**, 4439 (1998).
[17] A. Dreuw and M. Head-Gordon, J. Am. Chem. Soc. **126**, 4007 (2004).
[18] D. Tozer and N. Handy, Phys. Chem. Chem. Phys. **2**, 2117 (2000).
[19] M. Peach, P. Benfield, T. Helgaker, and D. Tozer, J. Chem. Phys. **128**, 044118 (2008).
[20] N. Maitra, J. Chem. Phys. **122**, 234104 (2005).
[21] J. Neugebauer, O. Gritsenko, and E. Baerends, J. Chem. Phys. **124**, 214102 (2006).
[22] N. Erickson and R. Holmes, J. Appl. Phys. **110**, 084515 (2011).
[23] P. Giannozzi, S. Baroni, N. Bonini, M. Calandra, R. Car, C. Cavazzoni, D. Ceresoli, G. Chiarotti, M. Cococcioni, I. Dabo, et al., J. Phys. Condens. Matter **21**, 395502 (2009).
[24] M. J. Frisch, G. W. Trucks, H. B. Schlegel, G. E. Scuseria, M. A. Robb, J. R. Cheeseman, G. Scalmani, V. Barone, B. Mennucci, G. A. Petersson, et al., *Gaussian09 Revision A.1*, gaussian Inc. Wallingford CT 2009.
[25] J. Perdew, K. Burke, and M. Ernzerhof, Phys. Rev. Lett **77**, 3865 (1996).
[26] D. Vanderbilt, Phys. Rev. B **41**, 7892 (1990).
[27] R. Bauernschmitt and R. Ahlrichs, Chem. Phys. Lett **256**, 454 (1996).
[28] M. Casida, C. Jamorski, K. Casida, and D. Salahub, J. Chem. Phys **108**, 4439 (1998).
[29] R. Stratmann, G. Scuseria, and M. Frisch, J. Chem. Phys **109**, 8218 (1998).
[30] C. Van Caillie and R. Amos, Chem. Phys. Lett **308**, 249 (1999).
[31] C. Van Caillie and R. Amos, Chem. Phys. Lett. **317**, 159 (2000).
[32] F. Furche and R. Ahlrichs, J. Chem. Phys **117**, 7433 (2002).
[33] G. Scalmani, M. Frisch, B. Mennucci, J. Tomasi, R. Cammi, and V. Barone, J. Chem. Phys **124**, 094107 (2006).
[34] A. Becke, J. Chem. Phys **98**, 1372 (1993).
[35] C. Lee, W. Yang, and R. Parr, Phys. Rev. B **37**, 785 (1988).
[36] Y. Zhao and D. Truhlar, Theor. Chem. Acc. **120**, 215 (2008).
[37] V. Anisimov, J. Zaanen, and O. Andersen, Phys. Rev. B **44**, 943 (1991).
[38] V. Anisimov, I. Solovyev, M. Korotin, M. Czyżyk, and G. Sawatzky, Phys. Rev. B **48**, 16929 (1993).
[39] I. Mazin and V. Anisimov, Phys. Rev. B **55**, 12822 (1997).
[40] M. Cococcioni and S. De Gironcoli, Phys. Rev. B **71**, 35105 (2005).
[41] V. Campo Jr and M. Cococcioni, J. Phys. Condens. Matter **22**, 055602 (2010).
[42] A. Kokalj, Comp. Mater. Sci. **28**, 155 (2003).
[43] R. Van Leeuwen and E. Baerends, Phys. Rev. A **49**, 2421 (1994).
[44] I. Vasiliev and R. Martin, Phys. Rev. A **69**, 052508 (2004).
[45] O. Gritsenko and E. Baerends, J. Chem. Phys. **121**, 655 (2004).
[46] Y. Tawada, T. Tsuneda, S. Yanagisawa, T. Yanai, and K. Hirao, J. Chem. Phys. **120**, 8425 (2004).
[47] M. Rohrdanz, K. Martins, and J. Herbert, J. Chem. Phys. **130**, 054112 (2009).
[48] J. Song, M. Watson, and K. Hirao, J. Chem. Phys. **131**, 144108 (2009).
[49] F. Della Sala and A. Görling, Int. J. Quantum Chem. **91**, 131 (2003).
[50] D. Jacquemin, E. Perpète, G. Scuseria, I. Ciofini, and C. Adamo, J. Chem. Theory Comput. **4**, 123 (2008).
[51] T. Stein, L. Kronik, and R. Baer, J. Am. Chem. Soc. **131**, 2818 (2009).
[52] T. Stein, L. Kronik, and R. Baer, J. Chem. Phys. **131**, 244119 (2009).
[53] N. Kuritz, T. Stein, R. Baer, and L. Kronik, J. Chem. Theory Comput. (2011).
[54] C. Hu, O. Sugino, and Y. Miyamoto, Phys. Rev. A **74**, 032508 (2006).
[55] C. Hu and O. Sugino, J. Chem. Phys **126**, 074112 (2007).
[56] T. Ziegler, A. Rauk, and E. Baerends, Theor. Chem. Acc. **43**, 261 (1977).
[57] T. Ziegler, Chem. Rev. **91**, 651 (1991).
[58] I. Frank, J. Hutter, D. Marx, and M. Parrinello, J. Chem. Phys. **108**, 4060 (1998).

[59] J. Behler, K. Reuter, and M. Scheffler, Phys. Rev. B **77**, 115421 (2008).
[60] J. Behler, B. Delley, S. Lorenz, K. Reuter, and M. Scheffler, Phys. Rev. Lett. **94**, 36104 (2005).
[61] M. Alducin, H. Busnengo, and R. Muiño, The Journal of chemical physics **129**, 224702 (2008).
[62] R. Maurer and K. Reuter, J. Chem. Phys. **135**, 224303 (2011).
[63] M. Levy and Á. Nagy, Phys. Rev. Lett **83**, 4361 (1999).
[64] P. Ayers and M. Levy, Phys. Rev. A **80**, 012508 (2009).
[65] L. Fritsche, Phys. Rev. B **33**, 3976 (1986).
[66] J. Cordes and L. Fritsche, Z. Phys. D **13**, 345 (1989).
[67] E. Gross, L. Oliveira, and W. Kohn, Phys. Rev. A **37**, 2805 (1988).
[68] E. Gross, L. Oliveira, and W. Kohn, Phys. Rev. A **37**, 2809 (1988).
[69] L. Oliveira, E. Gross, and W. Kohn, Phys. Rev. A **37**, 2821 (1988).
[70] W. Kohn, Phys. Rev. A **34**, 737 (1986).
[71] H. Kulik and N. Marzari, J. Chem. Phys **134**, 094103 (2011).
[72] A. Belozerov, M. Korotin, V. Anisimov, and A. Poteryaev, Phys. Rev. B **85**, 045109 (2012).
[73] M. Baldo, C. Adachi, and S. Forrest, Phys. Rev. B **62**, 10967 (2000).
[74] K. Goushi, R. Kwong, J. Brown, H. Sasabe, and C. Adachi, J. Appl. Phys **95**, 7798 (2004).
[75] S. Eom, Y. Zheng, E. Wrzesniewski, J. Lee, N. Chopra, F. So, and J. Xue, Appl. Phys. Lett **94**, 153303 (2009).
[76] C. Adachi, R. Kwong, and S. Forrest, Org. Electron. **2**, 37 (2001).
[77] T. Tsuboi and M. Tanigawa, Thin Solid Films **438**, 301 (2003).
[78] S. Lamansky, P. Djurovich, D. Murphy, F. Abdel-Razzaq, H. Lee, C. Adachi, P. Burrows, S. Forrest, and M. Thompson, J. Am. Chem. Soc. **123**, 4304 (2001).
[79] T. Hofbeck and H. Yersin, Inorg. Chem. (2010).
[80] M. Colombo, T. Brunold, T. Riedener, H. Guedel, M. Fortsch, and H. Buergi, Inorg. Chem. **33**, 545 (1994).
[81] A. Tsuboyama, H. Iwawaki, M. Furugori, T. Mukaide, J. Kamatani, S. Igawa, T. Moriyama, S. Miura, T. Takiguchi, S. Okada, et al., J. Am. Chem. Soc. **125**, 12971 (2003).
[82] W. Holzer, A. Penzkofer, and T. Tsuboi, Chem. Phys. **308**, 93 (2005).
[83] K. Ichimura, T. Kobayashi, K. King, and R. Watts, J. Phys. Chem. **91**, 6104 (1987).
[84] M. Baldo, C. Adachi, and S. Forrest, Phys. Rev. B **62**, 10967 (2000).
[85] P. Djurovich, E. Mayo, S. Forrest, and M. Thompson, Org. Electron. **10**, 515 (2009).
[86] K. Seki and K. Kanai, Mol. Cryst. Liq. Cryst **455**, 145 (2006).
[87] D. Cahen and A. Kahn, Adv. Mater. **15**, 271 (2003).
[88] A. Smith, M. Riley, S. Lo, P. Burn, I. Gentle, and B. Powell, Phys. Rev. B **83**, 041105 (2011).
[89] B. DAndrade, S. Datta, S. Forrest, P. Djurovich, E. Polikarpov, and M. Thompson, Org. Electron. **6**, 11 (2005).
[90] P. Hay, J. Phys. Chem. A **106**, 1634 (2002).
[91] K. Świderek and P. Paneth, J. Phys. Org. Chem. **22**, 845 (2009).
[92] E. Jansson, B. Minaev, S. Schrader, and H. Agren, Chem. Phys. **333**, 157 (2007).
[93] A. Kukhta, I. Kukhta, S. Bagnich, S. Kazakov, V. Andreev, O. Neyra, and E. Meza, Chem. Phys. Lett. **434**, 11 (2007).
[94] T. Hofbeck and H. Yersin, Inorg. Chem. **49**, 9290 (2010).
[95] K. Tang, K. Liu, I. Chen, et al., Chem. Phys. Lett. **386**, 437 (2004).
[96] B. Himmetoglu, R. M. Wentzcovitch, and M. Cococcioni, Phys. Rev. B **84**, 115108 (2011).
[97] T. Tsuboi, H. Murayama, S. Yeh, M. Wu, and C. Chen, Opt. Mater. **31**, 366 (2008).
[98] C. Adachi, R. Kwong, P. Djurovich, V. Adamovich, M. Baldo, M. Thompson, and S. Forrest, Appl. Phys. Lett. **79**, 2082 (2001).
[99] R. Holmes, S. Forrest, Y. Tung, R. Kwong, J. Brown, S. Garon, and M. Thompson, Appl. Phys. Lett. **82**, 2422 (2003).
[100] S. Tokito, T. Iijima, Y. Suzuri, H. Kita, T. Tsuzuki, and F. Sato, Applied physics letters **83**, 569 (2003).
[101] Y. You and S. Park, J. Am. Chem. Soc. **127**, 12438 (2005).
[102] H. Lee, Y. Hsu, T. Chen, J. Chen, K. Chen, and J. Wang, Inorg. Chem. **48**, 1263 (2009).
[103] F. De Angelis, S. Fantacci, N. Evans, C. Klein, S. Zakeeruddin, J. Moser, K. Kalyanasundaram, H. Bolink, M. Grätzel, and M. Nazeeruddin, Inorg. Chem. **46**, 5989 (2007).
[104] S. Lo, C. Shipley, R. Bera, R. Harding, A. Cowley, P. Burn, and I. Samuel, Chem. Mater. **18**, 5119 (2006).
[105] S. Su, E. Gonmori, H. Sasabe, and J. Kido, Adv. Mater. **20**, 4189 (2008).
[106] B. D'Andrade and S. Forrest, Adv. Mater. **16**, 1585 (2004).
[107] B. D'Andrade, R. Holmes, and S. Forrest, Adv. Mater. **16**, 624 (2004).
[108] H. Yersin, *Highly efficient OLEDs with phosphorescent materials* (Wiley Online Library, 2008).
[109] A. Jacko, B. Powell, and R. McKenzie, J. Chem. Phys. **133**, 124314 (2010).
[110] A. Jacko and B. Powell, Chem. Phys. Lett. **508**, 22 (2011).
[111] J. Slater, *The self-consistent field for molecular and solids, quantum theory of molecular and solids, vol. 4* (1974).
[112] E. Gross and R. Dreizler, *Density functional theory*, vol. 337 (Springer, 1995).